Displays 90 (2025) 103124

Contents lists available at ScienceDirect

Displays

journal homepage: www.elsevier.com/locate/displa

An optimized, color-adaptive blue light filtering approach using a novel color space transformation☆

Juan Bayón *, Joaquín Recas, María Guijarro

Department of Computer Architecture and Automatics, Complutense University of Madrid, Complutense avenue, Madrid, 28040, Madrid, Spain

ARTICLE INFO

Dataset link: https://www.kaggle.com/datasets/juanbayonfernandez/landscape-test-images

Keywords:
Computer vision
Blue filter
Blue light hazard
Color
Image processing
Spectral emission measure

ABSTRACT

Wearable screens are part of everyday life, but the blue light they emit can affect the human body. Known as the Blue Hazard, high-energy blue light has been linked to circadian rhythm disruption, reduced focus, cognitive functions, and Computer Vision Syndrome. As screens move closer to the eyes, especially in users with pre-existing eye conditions, effective filtering becomes increasingly important.

This work presents a blue light filter that processes images in a novel color space, selectively reducing high-energy pixels while preserving most colors. After filtering, both contrast and image quality remain virtually unchanged, according to several widely used metrics.

Physical measurements showed that blue light absorption exceeded theoretical expectations. Spectrophotometric tests across various screens demonstrated consistent performance—typically reducing 30%–40% of blue light for a color difference (ΔE) of 10, with absorption reaching up to 100%. Compared to f.lux and Night Shift, our filter reduces blue emissions by 17% and 34% more, respectively. With an average processing time of 0.012 s per image using basic parallelization (up to 85 Hz), it is well-suited for modern wearable and electronic devices.

1. Introduction

Wearables have become an integral part of daily life, ranging from watches to augmented and virtual reality devices. As the sector continues to grow, these devices are now used for a wide range of tasks, with screens featuring increasingly high resolutions. Notably, in the case of augmented and virtual reality, these screens are positioned directly over the eyes, raising concerns about their potential impact to our vision.

Blue light, the most energetic portion of the visible spectrum emitted by screens, has been extensively studied due to its potential links to various health issues [1–3], including macular degeneration, cancer, skin damage, and cataracts. Laboratory studies have demonstrated that blue light exposure can damage ocular tissues. Its danger in the context of everyday screen use remains a topic of debate.

Recent research reinforces concerns regarding the phototoxicity of blue light, specifically emitted by screens [4]. According to Haghani et al. [5], blue light emissions from electronic devices can disrupt circadian rhythms —known as artificial light at night (ALAN). Their systematic review links ALAN to several health conditions, including diabetes [6] and cancer [7–9]. Furthermore, a recent review published in Nature explores the impact of blue light on circadian regulation and beyond [10]. The authors note that blue light can affect cognitive and physiological functions independently of circadian processes, primarily through intrinsically photosensitive retinal ganglion cells (ipRGCs). These cells have been shown to influence brain regions responsible for attention, learning, memory, and executive function. As such, blue light plays a significant biological role, and both the quantity and timing of exposure are meaningful factors that should be carefully controlled.

As screens become brighter and are placed closer to the eyes, the potential hazards may be amplified. Devices such as augmented and virtual reality headsets, which are positioned directly in front of the eyes, often lack built-in filtering mechanisms. Consequently, the intensity of exposure – directly related to viewing distance – is higher, particularly during extended use. This is especially relevant for users who rely on these technologies intensively. In addition, head-mounted displays are increasingly being used as assistive devices for individuals with visual impairments or low vision [11]. The risks of the blue light are particularly pronounced in individuals with pre-existing conditions, such as low vision or other forms of ocular damage [12]. Many of these users rely on physical blue filters in their daily lives. Incorporating blue light filtering functionality directly into assistive devices not only enhances usability but also better aligns with the specific needs of

☆ This paper was recommended for publication by Guangtao Zhai.

* Corresponding author.
E-mail address: jbayon01@ucm.es (J. Bayón).

https://doi.org/10.1016/j.displa.2025.103124
Received 24 February 2025; Received in revised form 22 May 2025; Accepted 15 June 2025
Available online 4 July 2025

these users. In such scenarios, the implementation of effective blue light filtering becomes even more relevant.

To address these concerns, most commercial devices employ two primary strategies: dark modes in graphical interfaces and filtering technologies. While dark modes offer several benefits [13,14], they are unsuitable for video and image content. Consequently, filtering systems have emerged as the preferred approach for general applications, and they are the focus of our work. One of the earliest filtering systems was the f.lux project [15], followed by other examples like Eye Care for Android devices [16] and Night Shift for Apple products [17]. Studies analyzing various devices and their filtering systems [18–20] demonstrate that these technologies reduce blue light emissions by altering the overall color profile of images.

The widespread adoption of filtering systems is motivated not only by the need for ocular protection but also by the broader effects of blue light on human physiology. Blue light influences circadian rhythms through photosensitive retinal ganglion cells (ipRGCs), which play a crucial role in regulating the sleep-wake cycle [21]. Artificial stimulation of ipRGCs by screen exposure can disrupt these cycles, leading to sleep disturbances [22]. Additionally, blue light has been associated with visual fatigue, commonly referred to as Computer Vision Syndrome [23–25]. Other studies suggest links between blue light exposure and reduced memory capacity [26] or altered hunger regulation [17]. On the other hand, blue light has been shown to enhance alertness and dynamic vision [27], often to the detriment of other cognitive and physiological functions.

The primary contribution of our work is the development of a hardware-independent blue light filtering solution. Our filter can operate on any device, regardless of its underlying architecture. It can be implemented in augmented and virtual reality headsets, which typically lack built-in filtering mechanisms. These devices are key components in assistive systems for individuals with visual impairments, who can benefit from a software-based blue light filtering algorithm.

We propose a novel blue light filtering method that selectively targets the most energetic parts of an image by transforming it into a color space with a reduced rendering volume. The filter achieves excellent absorption rates while preserving most colors, contrast, and overall image quality. We demonstrate its efficiency through physical measurements of light emission: spectrophotometric analysis across various screens shows that our filter outperforms existing solutions and theoretical expectations.

This article is organized into six sections. Section 1 provides the introduction. In Section 2, we discuss the representation of color. Section 3 details the volumetric approach underlying the proposed filter. Section 4 describes the specifics of the filtering method. The results are presented in Section 5. Finally, Section 6 summarizes our conclusions, highlights the study's limitations, and suggests directions for future research.

2. Color and its spatial representation

Color is a fundamental component of human vision. We perceive color through specialized receptors in the retina, known as cones. These cones are divided into three types, each sensitive to one of the primary colors: red, green, and blue. The combination of signals from these cones allows us to perceive the wide range of colors in our environment. If we represent this perception in a three-dimensional coordinate system, with each axis corresponding to one of the primary colors, the resulting volume encompasses the possible combinations and colors. This volume forms a cube, representing the *RGB* color space. Similarly, digital displays use three emitters per pixel to simulate colors, each emitter corresponding to the intensity of one type of cone.

However, reducing the biological process of color perception to a set of coordinates oversimplifies reality—color also carries emotional and psychological significance [28]. It is well established that the number of colors humans can perceive exceeds those represented in the *RGB* space, as intermediate colors arise from combinations that cannot be fully represented by the three primary components. To address this limitation, alternative color spaces with different volumes have been developed, such as CIELAB and CIELUV [29]. These models offer a more accurate and homogeneous representation of colors, aligning more closely with human vision.

The evolution of color representation extends to display technologies, which strive to produce the widest possible range of colors. This range, known as the gamut, defines the volume of colors a display can reproduce. Standards such as REC.2020 and Adobe RGB [30, 31] provide expanded gamuts that surpass traditional *RGB* in color representation.

Regardless of the screen's gamut, this work focuses on reducing the volume associated with the most energetic colors, primarily blue and violet. Fig. 1 illustrates this process. The first row displays the original image, with the filtered result shown in the second row. Fig. 1b presents the *RGB* cube, highlighting the volume reduction. This reduction is more clearly appreciated in the side projection of the cube, shown in Fig. 1c. The blue and violet components are translated downward, reshaping the cube into a cone. Fig. 1d depicts the *xy* plane, a widely used format in colorimetric representation, where the cube is visualized as a triangle. In this plane, the blue corner coordinates shift towards the other vertices. These visualizations were generated using Kei Otsuka's Color Distribution Plotter [32], which is publicly available on Matlab Central.

The proposed filter reduces the spatial representation of colors by approximating the cube to a cone. This new color space, termed *RGb*, is introduced in this work, where the lower-case *b* represents the reduced blue component. The filter computes this space and converts the coordinates into the new color space, effectively diminishing the emissions of the most energetic colors. In the *RGb* space, the diagonal corresponds to grayscale or luminance, which is preserved. Colors above the diagonal, characterized by a high blue component, are transformed into adjacent colors in the spectrum towards the diagonal. We detail the calculation of the *RGb* color space in the following section.

3. Filter approach

Filtering using the color space as a tool involves reducing the volume of color representation in an image. The greater the reduction in volume associated with short wavelengths, the lower the resulting energy emission. However, excessive volume reduction leads to fewer colors being represented, diminishing the realism of the image. The proposed filter addresses this challenge by seeking an optimal balance between two factors: the blue emission B_e and the representation volume, or gamut G.

B_e represents the proportion of blue remaining in the Blue channel of the image, defined as the ratio of the remaining blue to its original amount. G_{diff} denotes the difference in representation volume between the original and filtered images. The representation volume is normalized to a maximum value of one unit, irrespective of the number of colors it encompasses. Consequently, both metrics are expressed on the same scale, ranging from zero to one, but with opposite interpretations: B_e indicates the proportion of blue retained, which decreases as the representation volume difference, G_{diff}, increases.

The objective is to reduce the representation volume sufficiently to optimize absorption while maintaining an acceptable level of image quality. This trade-off is framed as a cost function that balances the blue emission (B_e) and the gamut difference (G_{diff}). A lower gamut corresponds to higher absorption, but excessive reduction can compromise the image's realism. The optimal filter for a given screen is determined by minimizing the absolute difference between these two normalized values, as they are inversely related but not directly proportional. Additionally, a quality control factor, Q, ensures that image quality is preserved throughout the transformation process. Under ideal conditions, this factor approaches zero, indicating that quality is maintained.

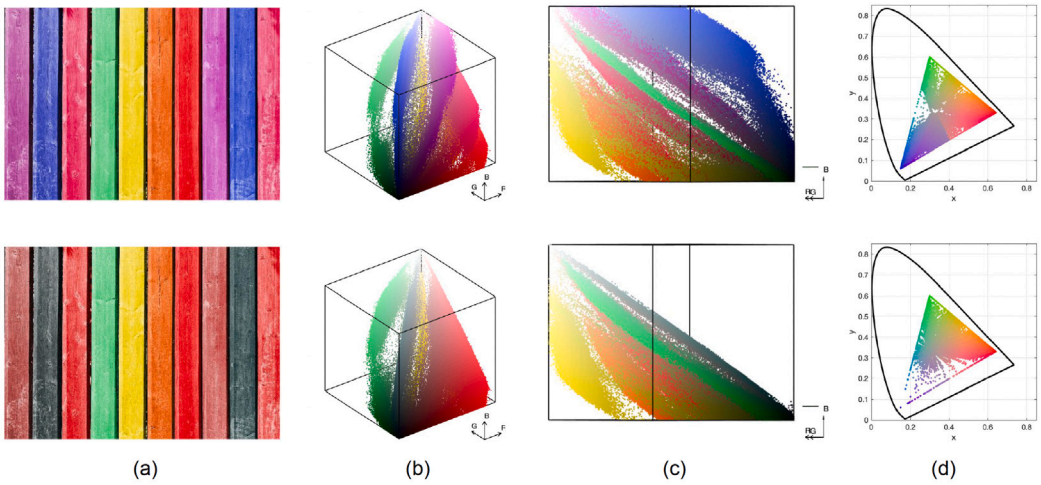

Fig. 1. Filter functioning example and its volumetric color representation.

When image realism is at risk, Q adjusts the cost function to prioritize quality. Therefore, Eq. (1) defines the cost.

$$cost = |B_a - G_{diff} - Q| \tag{1}$$

Quality measures for multimedia files are diverse. In this work, we use three non-referential metrics, meaning they do not directly compare the filtered image with the original. Among them, one represents the observer's opinion and the other two are reportedly objective in a supervised and unsupervised manner. These three metrics are well known in the scientific literature, to the point of being included in some programming languages: Brisque [33] (B), Piqe [34] (P), and Nique [35] (N). Eq. 7 calculates the quality term, where the subscript 0 represents the original quality and the subscript f denotes the value after filtering. It comprises three quality terms, one corresponding to each metric. When the metric values before and after filtering are identical, each term equals one. Therefore, when quality is fully preserved, the sum of the filtered metrics equals minus three, resulting in Q being zero.

$$Q = 3 - B_f/B_0 - N_f/N_0 - P_f/P_0 \tag{2}$$

To increase absorption, the color representation volume must be reduced. However, to preserve as much of the total volume as possible, modifications should be limited to pixels with an excess of blue. Changing the color space involves a linear transformation of the three primary color components, which alters the representation volume. In alternative color spaces to *RGB*, the blue component is part of at least one of the color coordinates and is compensated by the other two, enabling the selection of pixels with a predominant blue component.

Color spaces such as *YES*, *YIQ*, or *YUV* include a blue channel that can be leveraged for filtering. For instance, in the *YES* color space, the S channel is defined as $S = 0.25R + 0.25G - 0.5G$. Negative values of S correspond to pixels where the proportion of blue exceeds that of red and green combined. Building on this approach, we propose a linear transformation adapted to the image, selecting the appropriate proportions of each color. The coefficient matrix F_c is defined by the color coefficients f_{c1} and f_{c2}, which scale the primary colors. The matrix transformation T is computed as the product of each pixel and the coefficient matrix F_c. Algorithm Eq. (3) provides the formal representation.

$$T = RGB * F_c = RGB * \begin{bmatrix} -f_{c1} \\ -f_{c2} \\ f_{c1} + f_{c2} \end{bmatrix} \tag{3}$$

T defines a surface that acts as a new boundary for the color space, reducing its height, which corresponds to the blue component. Each pixel's T value represents the coordinate translation necessary to achieve the desired volume reduction. Fig. 2 conceptually illustrates this process, with the shape exaggerated for clarity. In the figure, the transformation of a pixel P is represented as $T(P)$. Positive T values indicate an excess of blue and determine the magnitude of the translation vector, while T values less than zero result in no translation, as the pixel already lies within the new volume.

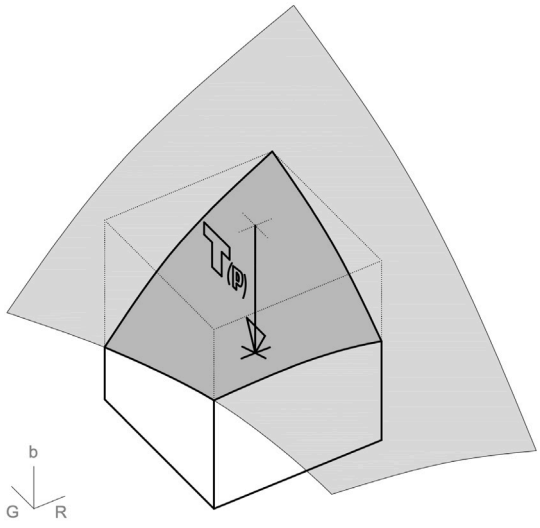

Fig. 2. Transformation of the RGB cube into the RGb cone.

In the new reduced-volume color space, *RGb*, the *Red* and *Green* components remain constant, while b is determined as the B coordinate applying the vertical translation. As shown in the figure, the cube gradually transforms into a cone, with its generatrix approximately aligning along the diagonal. This diagonal represents the white-to-black gradient, corresponding to luminance.

The problem we address is the optimization of the color coefficients, f_{c1} and f_{c2} to minimize the cost function, using a gradient descent algorithm. These two factors define the cutting edge of the new volume, removing the maximum amount of blue with the least possible reduction. Additionally, by maintaining the diagonal of the cube, the resulting filter ensures that contrast is preserved.

The optimal filter determines the values of f_{c1} and f_{c2} within the range of $[-1, 0.5]$. The column matrix F_c has a sum of zero, which is inherent in its definition. This ensures equilibrium among the primary colors and aligns the cutting limit along the cube's diagonal. The blue

component must be constrained to positive values between 0.5 and 1.0 to ensure that the filter consistently reduces blue intensity.

The theoretical framework of this process leads to several interesting conclusions, which are applied to the design of the filtering process. These details are elaborated in the following section.

4. Proposed filter

Using gradient descent to minimize the cost, we determine the optimal transformation to the new *RGb*, obtaining values for f_{c1} and f_{c2}. We tested the process with numerous images and found that most cases can be simplified into four distinct scenarios that closely approximate the optimal output. Consequently, the process can be reduced to a search among these four cases rather than an optimization. Each scenario is defined by its coefficient matrix F_c: (a) $[-1.0, 0.5, 0.5]$; (b) $[0.5, -1.0, 0.5]$; (c) $[0.0, -1.0, 1.0]$; (d) $[-1.0, 0.0, 1.0]$. These cases represent boundary conditions where one of the primary colors is maximized while the other components provide compensation. Simplifying the process results in improved execution, determining which of these cases is most suitable for a given image based on its dominant color composition.

The most efficient coefficient matrix F_c in terms of blue absorption, corresponds to the matrix transformation T that accumulates the highest sum of positive values. By calculating this sum in advance, we can identify the most effective filter. However, in some cases, the simplification may result in a color difference greater than desired by the user. To address this, we introduce a correction factor based on ΔE.

The color difference, ΔE, is the Euclidean distance in the *CIE* $L^*a^*b^*$ color space, a standard metric widely used in the scientific literature [36]. We define the color difference between the original and filtered images as the average Euclidean distance across all pixels. Due to the subjective nature of the correction factor, which adapts to user perception, extreme precision is not necessary. To simplify the computation, we approximate the Euclidean distance in the *RGB* color space. Therefore, the Euclidean distance for one pixel is the modulus of the vector connecting the pixel $RGB_{original}$ with $RGB_{filtered}$, as expressed in Eq. (4).

$$((R_0 - R_t)^2 + (G_0 - G_t)^2 + (B_0 - B_t)^2)^{1/2} \tag{4}$$

The translation we propose has only a vertical component by definition, modifying the blue coordinate. The red and green differences in the equation are zero because these components remain unchanged. Simplifying, $\Delta E = ((B_0 - B_t)^2)^{1/2}$, which further reduces to $\Delta E = B_0 - B_t$. Hence, when measured in the *RGB* color space, ΔE directly corresponds to the value of the matrix transformation T, which is already known. The average value of T represents the overall color difference for the filtered image, denoted as ΔE_{image}. In other words, the color difference is the result of the filter, represented by T.

In our filter design, the user provides ΔE_{user}, which is used to regulate filter effectiveness. When ΔE_{user} is negative, its absolute value is the filter limit, preventing unrealistic color differences. When positive, it enhances the filter's effect, allowing up to nearly 100% blue light reduction. If ΔE_{user} is zero, neither enhancement nor limitation is applied. The parameter ΔE_{user} ranges from −100 to 100. Specifically, a value of $\Delta E_{user} = -100$ results in no filtering, while $\Delta E_{user} = 100$ applies the maximum filtering level.

We use ΔE_{user} to calculate the correction factor f_c as the ratio of the color difference in the filtered image: $f_c = \Delta E_{user}/\Delta E_{image}$. f_c scales T to limit or enhance the transformation. For positive values of f_c, we multiply T by $1 + f_c$, to increase the translation. For negative values, we use its absolute value as a limit, ensuring a minimum effectiveness of 0.3. This limit is only applied when the filtered image exhibits a greater color difference than desired.

The resulting filter is detailed in Algorithm 1. The filter dynamically adjusts the reduction of blue light emissions based on the user's specified regulation, adapting to their needs and preferences. The proposed filtering mechanism is both adaptive and customizable, offering flexible, user-centered control over blue light exposure—ranging from no filtering to the maximum reduction achievable by the algorithm.

Algorithm 1 Filter

inputs: $image$, ΔE_{user}
outputs: $filteredImage$
$a \leftarrow [-1.0, 0.5, 0.5]$
$b \leftarrow [0.5, -1.0, 0.5]$
$c \leftarrow [0.0, -1.0, 1.0]$
$d \leftarrow [-1.0, 0.0, 1.0]$
$filters \leftarrow [a, b, c, d]$
$sums \leftarrow newList()$
$f_c \leftarrow 1$
for $filter\ in\ filters$ **do**
  $T \leftarrow image * filter$
  $T < 0 = 0$
  $sums.append(sum(T.RGB))$
end for
$bestIndex \leftarrow indexOfMaxValue(sums)$
$T = transformations[bestIndex]$
$\Delta E \leftarrow sums[bestIndex]$
if $\Delta E_{user} < 0$ & $\Delta E_{image} > |\Delta E_{user}|$ **then**
  $f_c = maxValue(0.3, \Delta E_{user}/\Delta E_{image})$
end if
if $\Delta E_{user} > 0$ **then**
  $f_c = 1 + |\Delta E_{user}|/\Delta E_{image}$
end if
$T = T * f_c$
$filteredImage[B] = image[B] - T$

The filter processes an image and computes the four possible matrix transformations T. It then calculates the sum of the positive values and selects the option with the highest sum. Subsequently, if ΔE_{user} is negative but still smaller than ΔE_{image}, a correction factor f_c is computed with a value ranging from 0.3 to nearly 1 to reduce the filter's effect. If ΔE_{user} is positive, f_c is increased by one to enhance the effect. Finally, the correction factor is applied to the matrix transformation T, and the translation is performed, generating the filtered image. In the following section, we analyze the outcomes in detail and provide results to illustrate the process.

5. Results

First, we present theoretical results on the filter's performance, and then we provide empirical results by directly measuring screen emissions. The results were obtained using MATLAB version R2023a, running on macOS Sonoma 14.3.1. The tests were conducted on a laptop equipped with a 2.4 GHz Intel Core i5 processor and 16 GB of RAM. The main dataset consisted of 100 images selected from the publicly available Landscapes dataset [37], which is distributed under a free license. These images were chosen to represent a wide range of colors and combinations [38].

Fig. 3 illustrates the filtering results using sample images that are predominantly pink, violet, and a mix of blue and white. The absorption is computed as the reduction in the blue channel of the *RGB* color space. The optimal filter, which is neither limited nor enhanced, is highlighted with a red box. From left to right, the sequence of images includes the original image, the filter limited to $+5\Delta E_{user}$, the optimal filter (boxed), the filter augmented by $+10\Delta E_{user}$, the filter augmented by $+40\Delta E_{user}$, and the filter augmented by $+100\Delta E_{user}$. The corresponding blue absorption percentages for each image, from left to right, are as follows: (1) Top image: 11%, 38%, 48%, 77% and 100%; (2) Middle image: 13%, 44%, 52%, 75% and 100%; (3) Bottom image: 8%, 27%, 32%, 45% and 73%. The filter preserves most colors,

Fig. 3. Effect of the filter on images with predominance of colors with great composition of blue.

Fig. 4. Different outcomes with different transformation matrices. On the left, the original image. On right, four filtered images using the four coefficient matrices F_c.

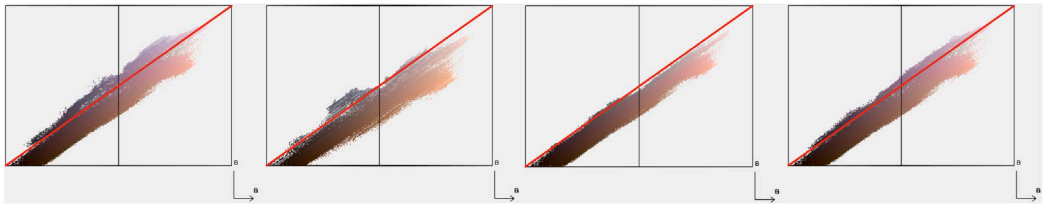

Fig. 5. *RGB* cube representation for the four coefficient matrices F_c.

modifying only those dominated by blue, such as blue and violet. As absorption increases up to 100%, the color difference also increases. The user can regulate the filter according to their needs, adjusting between realism and efficiency. For users with specific conditions, the filter can be adjusted to block nearly all blue light, providing a tailored solution. The optimal filter serves as a reference, providing a balanced trade-off between color difference and absorption. In all cases, white is preserved, maintaining contrast, as is clearly visible in the bottom image.

The filter selects the most appropriate transformation from four options, each represented by a different coefficient matrix F_c. The selected transformation is the one that best adapts to the image's color composition and removes the greatest amount of blue. Fig. 4 illustrates the outcomes of applying the four matrices to the same image. The largest image represents the original. Among the filtered images, the top-left ($a = [-1.0, 0.5, 0.5]$) performs poorly, failing to remove significant blue content, with a blue absorption of 1% and ΔE of 0,27. The bottom-right image ($d = [-1.0, 0.0, 1.0]$) also shows limited effectiveness, with blue absorption of 2% and ΔE of 1.60. The bottom-left image ($c = [0.0, -1.0, 1.0]$) alters the sky but leaves the mountains unchanged, with a blue absorption of 9% and ΔE of 6,09. Finally, the top-right image ($b = [0.5, -1.0, 0.5]$) is identified as optimal, as it effectively removes blue from both the sky and the mountains, with a blue absorption of 15% and ΔE of 10,12.

Fig. 5 displays the pixel representation within the *RGB* color space cube, from a lateral perspective. The red line represents the diagonal of the cube, corresponding to the black-to-white scale — black is located at the bottom-left vertex, while white is at the top-right. The arrangement of the cubes follows the same order as the photographs, progressing from top-left to bottom-right. The filter matrices are from left to right: *a*, *b*, *c*, and *d*. Among these, matrices *b* and *c* are the most effective. However, matrix *c* translates pixels directly towards the diagonal, resulting in a smaller representation volume. In contrast, matrix *b* distributes the pixels more broadly, preserving a higher representation volume with higher absorption. This broader distribution allows the image to retain a greater number of colors while still effectively reducing blue light. For this particular image, we conclude that matrix *b* is the optimal F_c.

By preserving the black-to-white diagonal, the filter ensures that contrast is maintained. Maintaining contrast is essential for preserving the accuracy of shape representation. Fig. 6 illustrates the contrast difference between the original and filtered images, evaluated using the Histogram Spread metric (*HS*) [39]. A more uniform histogram indicates better contrast, and the *HS* metric has been widely validated in scientific studies as a reliable measure of contrast quality [40].

The left panel of Fig. 6 shows the *HS* values for the 100 images in the dataset. Although the histogram spread is diverse across images, the filter demonstrates robustness, maintaining consistent *HS* values. The middle panel displays the contrast difference when using the optimal filter configuration, while the right panel shows the contrast difference with the filter enhanced to ΔE_{user} +100. In both cases, the

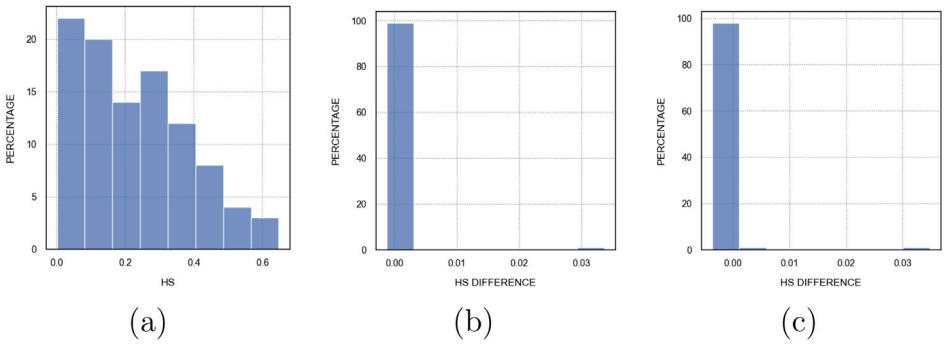

Fig. 6. Results of the filter using 100 images: (a) *HS* value for the 100 images; (b) HS difference with the optimal filter; (c)HS difference with filter amplified to ΔE +100.

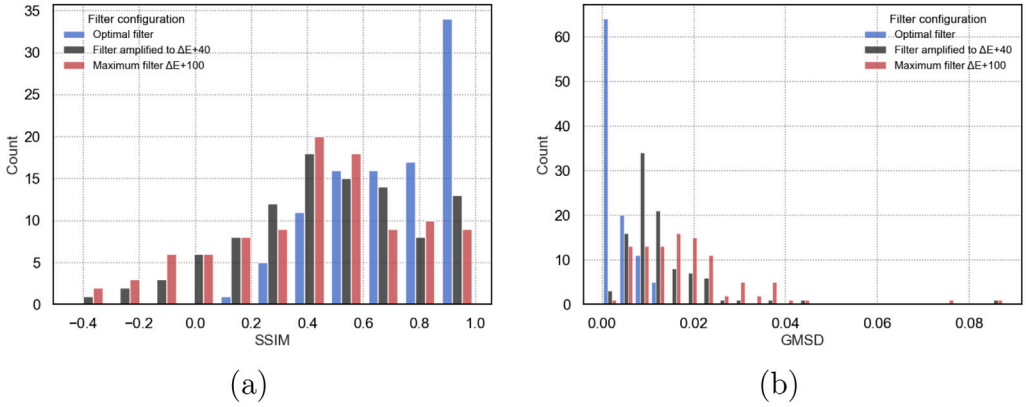

Fig. 7. Results of the filter using 100 images with different filter configurations: (a)SSIM; (b) GMSD.

contrast difference remains negligible, with values close to zero. These results confirm that our filter effectively preserves contrast, ensuring the integrity of shape representation and image details.

Image Quality Assessment (IQA) metrics are used to evaluate the perceptual quality of an image. We assessed the quality of our filter using the same set of 100 images. One of the most widely used metrics in the scientific literature is SSIM (Structural Similarity Index) [41], which considers luminance, contrast, and color differences, as shown in Fig. 7a. SSIM values range from 1 to −1, with 1 indicating identical images. Since SSIM incorporates color differences in its computation, the metric tends to decrease – and can even become negative – as the level of filtering enhancement increases. These results indicate that the filtered images differ in color from the originals, which is an expected effect of the filtering process. However, under the optimal filter configuration, most images tend to score close to 1, indicating high structural similarity.

Other quality metrics confirm that the visual structure of the images is preserved. Fig. 7b shows results for GMSD (Gradient Magnitude Similarity Deviation) [42], a metric specifically designed to detect image distortions. GMSD values range from 0 upward, with values below 0.05 indicating high similarity and minimal distortion. In our tests, 98 out of 100 images had a GMSD value below 0.05, and many returned zero, indicating that structural quality is largely unaffected by the filter.

We also present results using non-referential IQA metrics in Fig. 8, which assess image quality without comparison to the original. The three metrics – NIQE [35], BRISQUE [33], and PIQE [34] – are widely adopted and supported in many programming languages. The results are expressed as the difference between the quality scores of the original and filtered images. While there are minor fluctuations, the values remain very close to zero, supporting the conclusion that the filter preserves overall image quality.

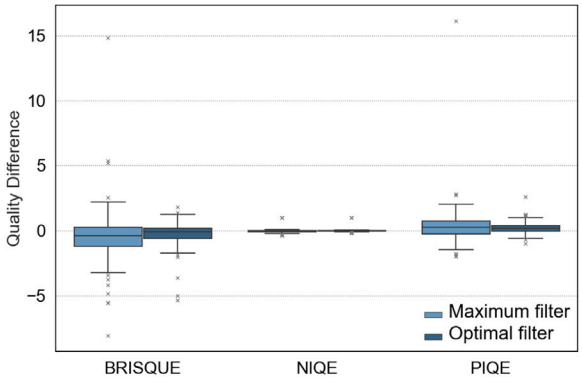

Fig. 8. IQA metrics: brisque, niqe, pique.

About the performance of the filter, Fig. 9 illustrates the absorption values (Fig. 9a), representation volume rate (Fig. 9b), and color difference (Fig. 9c) for various filter configurations. From left to right, each plot box corresponds to a filter configuration: ΔE_{user} of −5 (limited to 5), the optimal filter (without limitations or enhancements), and filters enhanced by $+10\Delta E_{user}$, $+40\Delta E_{user}$, and $+100\Delta E_{user}$. The volume reduction has an average of 15%, up to 36% with the optimal filter. With a ΔE_{user} limitation, absorption remains low but preserves realistic colors, with the color difference approaching zero and volume difference rate near one. The optimal filter configuration achieves blue light absorption typically ranging between 30% and 40%, providing the best balance between volume preservation and absorption. At medium enhancement of $+40\Delta E_{user}$, absorption increases to 60%, while color differences remain within acceptable limits. At the maximum enhancement of $+100\Delta E$, the color difference and representation volume

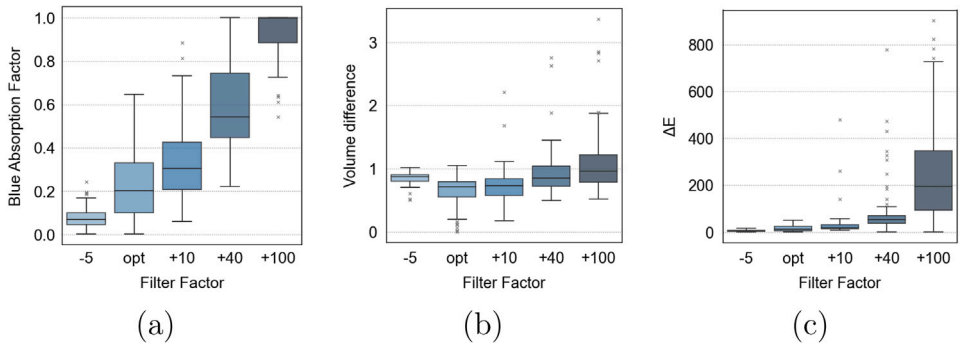

Fig. 9. Results of the filter using 100 images: (a) Blue absorption; (b) Volume difference with the new color space; (c) ΔE.

Fig. 10. Experiment setup.

difference significantly increase. Nevertheless, the filter achieves 100% blue light absorption in most cases.

Also Fig. 9 shows that with medium enhancement, the filter achieves high absorption levels. As the enhancement increases, the representation volume decreases, which is reflected in the color difference ΔE. However, this increase remains controlled for values up to +50 ΔE_{user}. When the filter is maximized, absorption typically reaches 100%, although the color difference rises significantly. In summary, the absorption ratio is considerable with controlled color differences in most cases, while the filter's customization allows users to adapt it to any circumstance even achieving total absorption when required.

The theoretical results demonstrate that the filter performs effectively, achieving significant blue light absorption while preserving most colors in the *RGb* color space at its maximum volume. To validate these findings, we tested the same set of 100 images using a spectrophotometer. Photometry was employed to quantitatively measure radiation and assess its potential impact on a human observer [43]. Fig. 10 illustrates the experimental setup.

The Ocean SR2 spectrophotometer was employed, modified with an entrance rack of 200 nanometers to accommodate screens of varying sizes, because the standard 50-nanometer rack is less sensitive for smaller screens. The device was calibrated in-house using Ocean View's UV calibration, paired with a 200-nanometer endpoint fiber. The fiber was positioned directly in front of the screen using a holder, and the room was completely darkened to ensure that the screen was the sole light source. The spectrophotometer outputs spectral intensity in counts, where each count corresponds to the number of photons detected at a given wavelength, measured in nanometers.

The experiment consists of a comparison between the original image and the filtered image under various filter configurations. To ensure a fair and consistent evaluation, all tests were conducted on the same laptop screen under identical lighting conditions, with the room darkened to eliminate ambient light interference. The spectrophotometer was positioned at the same distance, angle, and orientation for each measurement. The images were displayed in full-screen mode, occupying the same screen area and activating the same pixels. The sensor exposure time was fixed at 100 ms for all static images. As a result, the intensity measured at each wavelength is directly comparable across all configurations.

The noise was subtracted from the measurement and the screen irradiance was calculated using parameters from the calibration file, including the area of initial diffraction and other relevant metrics. All results are comparative, assessing the original image against the filtered image. The potential error from the setup and measurement device can be disregarded, as it remains consistent across comparisons. Consequently, standard deviation values are not reported, and conclusions are drawn directly from the measurements.

For the test, we used a 2009 MacBook Pro with a Retina display. The screen's color profile was set to "Color LCD", and brightness was adjusted to 80% of its maximum emission. Fig. 11 shows the visible spectrum irradiated under different filter configurations applied to the same image. The visible spectrum ranges from 380 nm to 750 nm, with the blue component spanning 400 nm to 495 nm. The measured images are shown below: (a) Original image; (b) Filter limited to $-5\Delta E$; (c) Optimal filter; (d) $+10\Delta E$ enhancement; (e) $+40\Delta E$ enhancement; (f) $+100\Delta E$ enhancement. As the filter's effectiveness increases, blue light absorption improves, with maximum absorption occurring at the 450 nm wavelength. Other wavelengths corresponding to non-blue colors remain largely unaffected, meaning most colors are preserved, except for bluish tones. At the maximum enhancement of $+100\Delta E$, the filter absorbs 69% of the 450 nm wavelength associated with blue light. The decision to maintain pure white ensures that contrast is preserved, even under these conditions, although it limits the overall absorption. With the optimal filter configuration, absorption reaches 35%, with a color difference of 23, achieving a balance between blue light reduction and color fidelity.

Fig. 12 illustrates the same experiment conducted with a violet-dominated image. With this color distribution, the filter achieves 100% absorption in the most enhanced configuration. In the case of the optimal filter, the absorption is lower than in the previous experiment, reaching 28%, but the color difference is only 10, resulting in a better absorption-to-color-difference ratio. When the filter is enhanced by

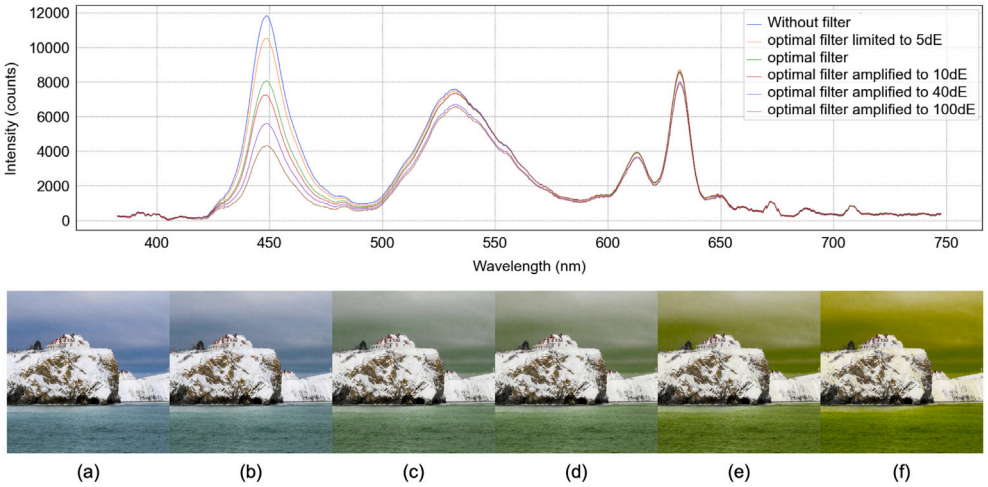

Fig. 11. Filter effect on a blue and white image: (a) Original image; (b) Filter limited to $-5\Delta E_{user}$, 12% absorption at wavelength 450, color difference of 7.00; (c) Optimal filter, 35% absorption, color difference of 23.56; (d) Filter amplified to $+10\Delta E_{user}$, 42% absorption, color difference of 29.28; (e) Filter amplified to $+40\Delta E_{user}$, 57% absorption, color difference of 44.19; (f) Filter amplified to $+100\Delta E_{user}$, 69% absorption, color difference of 55.68.

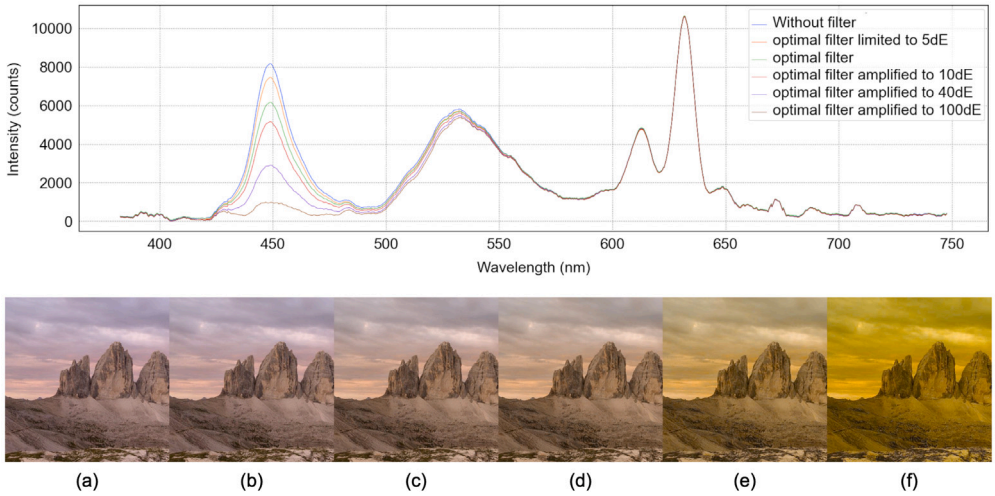

Fig. 12. Filter effect on a violaceous image: (a) Original image; (b) Filter limited to $-5\Delta E_{user}$, 10% absorption at wavelength 450, color difference of 3.16; (c) Optimal filter, 28% absorption, color difference of 10.12; (d) Filter amplified to $+10\Delta E_{user}$, 42% absorption, color difference of 15.84; (e) Filter amplified to $+40\Delta E_{user}$, 74% absorption, color difference of 31.96; (f) Filter amplified to $+100\Delta E_{user}$, 100% absorption, color difference of 51.06.

$+10\Delta E$, absorption rises to 42%, with a color difference of 15. These results demonstrate that the filter can achieve significant blue light absorption while maintaining low color differences.

Fig. 13 presents the results of the filtering process applied to a photograph containing a wide range of colors. The filter modifies only the blue components of the image while preserving the remaining colors. In this case, the optimal filter and the enhanced filter with $+10\Delta E_{user}$ achieve low color differences of 3.92 and 9.06, respectively, with absorption rates of 17% and 36%.

These examples collectively demonstrate that the filter achieves significant blue light absorption while altering only the most energetic colors, maintaining low color differences. The filter typically removes between 20% and 40% of blue light with a color difference around 10, which is considered a favorable outcome. For users requiring higher absorption levels, the filter's effectiveness can be enhanced up to 100%, at the cost of a higher color difference.

We tested the same 100-image dataset [38] with the spectrophotometer, now focusing on the 450 nm wavelength, which corresponds to the peak of blue light emission. Fig. 14 compares the theoretical absorption with the real absorption measured using the spectrophotometer for this wavelength. The real absorption of the screen emission exceeds theoretical expectations in most images across all configurations, except for the highest enhancement level, $+100\Delta E_{user}$. With the optimal filter, as well as with small to medium enhancements, the real absorption is greater than expected. However, when the filter reaches its maximum level, absorption becomes limited. Nonetheless, with slight enhancement, it is possible to achieve the maximum absorption while maintaining a balanced color difference. These results suggest that medium enhancements, particularly the optimal configuration, are the most recommended, as they offer a good trade-off between blue light reduction and color preservation. The spectrophotometer results confirm the effectiveness of the filter.

We compared our filter with existing solutions, including the free software f.lux for Mac and the Night Shift feature on iOS. Both systems modify the entire screen by shifting pixel colors towards orange. Images of their outputs are unavailable due to restrictions on screenshots imposed by these programs. However, original and filtered images for our approach are provided in Fig. 16. Fig. 15 illustrates the emission spectra for different configurations of f.lux and Night Shift. Our filter absorbs more than 90% of blue light, whereas Night Shift at its maximum setting absorbs 65%, and f.lux at a color temperature of 2700 K absorbs 82%. This represents an improvement of 34% over

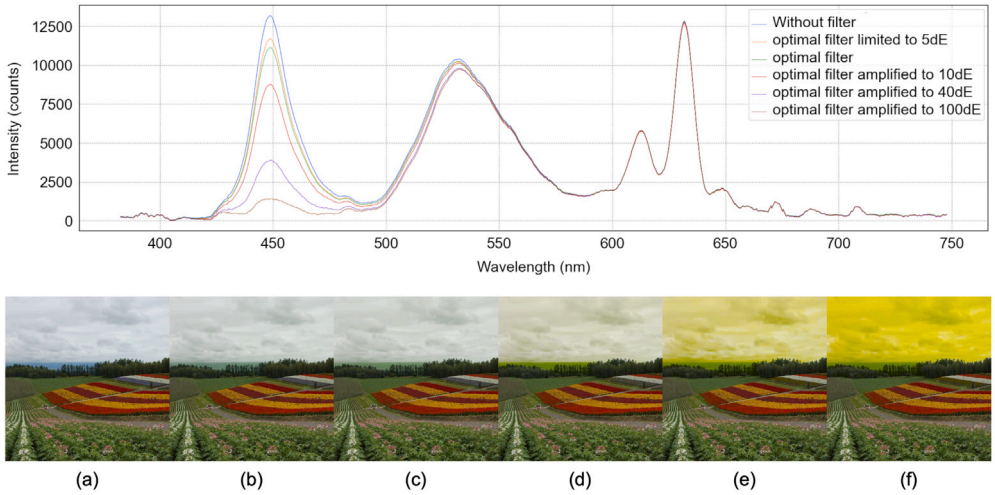

Fig. 13. Filter effect on different colors in the image: (a) Original image; (b) Filter limited to $-5\Delta E_{user}$, 12% absorption at wavelength 450, color difference of 2.86; (c) Optimal filter, 17% absorption, color difference of 3.92; (d) Filter amplified to $+10\Delta E_{user}$, 36% absorption, color difference of 9.06; (e) Filter amplified to $+40\Delta E_{user}$, 77% absorption, color difference of 22.00; (f) Filter amplified to $+100\Delta E_{user}$, 97%absorption, color difference of 33.35.

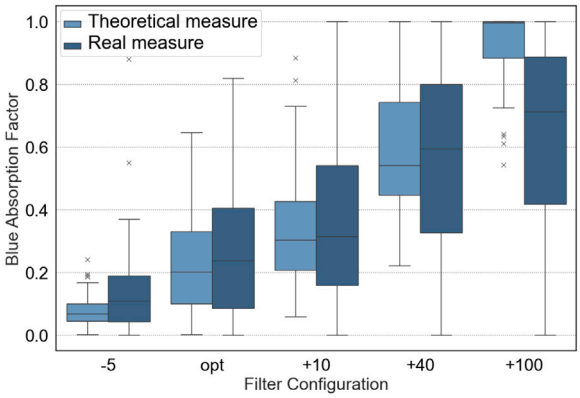

Fig. 14. Theoretical versus real absorption.

Night Shift and 17% over f.lux. Although full blue light absorption is not always necessary, our filter allows user-controlled modulation up to the maximum level, adapting to individual preferences and needs. These results highlight the effectiveness of our filter, showing that it can outperform existing solutions.

Additionally, Fig. 15 shows that both f.lux and Night Shift not only reduce blue light but also alter the green and red light projections, significantly increasing red emission. As a result, these filters change all colors in the image, whereas our approach selectively modifies only the most energetic blue components. The energy projection for high frequencies (e.g., red colors) in our filtered images remains nearly identical to that of the original image.

We tested the filter using the same image previously analyzed with f.lux and Night Shift across different devices and operating systems: iOS on an iPhone, Android on a smartphone, and Windows on a laptop. Fig. 17 presents the irradiance spectra for these cases, showing consistent outcomes. In all three scenarios, our filter achieved an absorption rate near 100%, comparable to the results from the MacBook tests, demonstrating that the filter's effectiveness is not tied to a specific screen type.

However, the emitted energy varies across devices, depending on the type of screen. Additionally, mobile screens are placed closer to the fiber during measurements to ensure accurate readings. Consequently, the absolute absorption values differ between devices, even though the filter's relative effectiveness remains consistent. Notably, on mobile devices (both Android and iOS), the filter induces slight changes in other colors, reducing green and red emissions when applied to the same image used on laptops. This effect was beyond the scope of this study and could be explored in future research.

The filter was tested on the MacBook Pro using the full set of 100 images, achieving an average processing time of 6.90 s in total, or approximately 0.069 s per image, without parallelization. The average processing time was calculated using MATLAB's native timing function, which executes the code multiple times with a high-resolution timer. By simply calculating the four transformations in parallel to select the optimal, the algorithm processes the 100 images in just 1.1796 s, or approximately 0.012 s per image. This corresponds to a refresh rate of 85 Hz, which is compatible with many modern displays. Since pixel processing is completely independent, the algorithm exhibits a high degree of extra parallelism and there is room for improvement in future work. These results are promising and suggest that the filter could be effectively applied in electronic devices and wearable technologies.

6. Conclusions, limitations and future work

Blue light affects the human body in various ways, making the control of its emission from electronic devices a topic of significant interest. This work proposes a filter that reduces the color representation volume for image projections, absorbing approximately 40% of blue light in its optimal configuration with a color difference of around 10. The filter's effectiveness can be further enhanced by user customization, achieving up to 100% absorption at the cost of a higher color difference.

The results were obtained through direct physical measurements of screen emissions. We tested the filter using a spectrophotometer, and the real absorption surpasses the theoretical predictions, achieving excellent results across different devices. Absorption rates are consistent between different screen types up to the maximum absorption of 100%. Moreover, when compared to previous solutions, our filter demonstrates superior performance in the blue light emission, with an improvement of 34% over Night Shift and 17% over f.lux.

The filter leverages an alternative color space that dynamically adapts to the image's color distribution to optimize performance. With an average reduction of 15% volume representation, the filter achieves an average blue absorption of 43%. Additionally, it preserves contrast, image quality, and the overall color appearance. The contrast difference, measured using the histogram spread metric, is effectively zero in most cases. Similarly, image quality is maintained, with differences tending towards zero across multiple evaluation metrics, including GMSD, NIQE, BRISQUE, and PIQE.

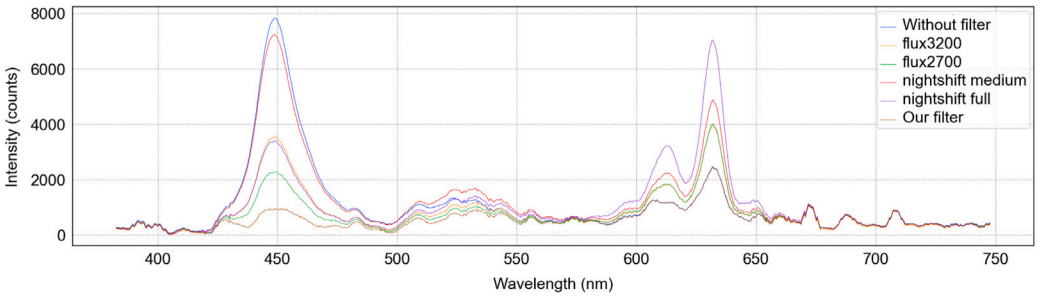

Fig. 15. Effect of different filters compared with our solution.

(a) Original image (b) Optimal filter

Fig. 16. Result of the optimal filter with a predominantly violet image.

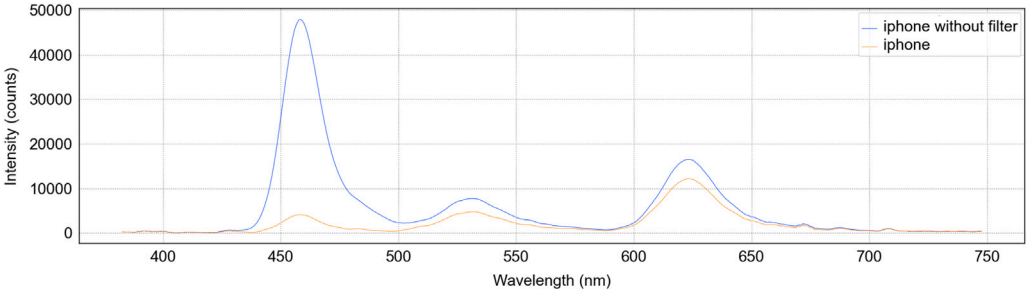

(a) Image projected in the iOS device Iphone Pro Max 14 without filter and with our optimal filter.

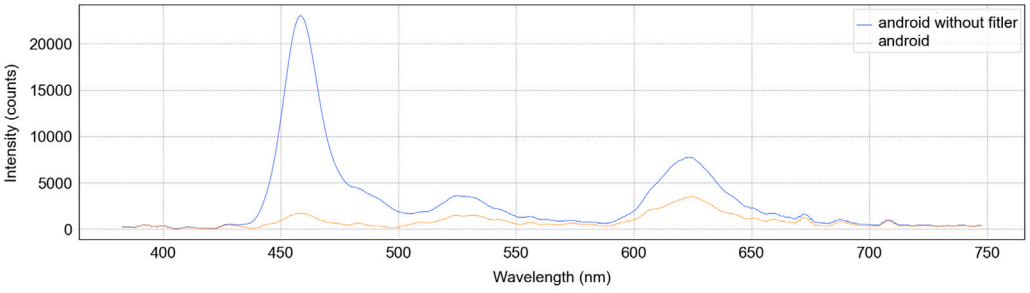

(b) Image projected in the Android device Oppo Find X5 without filter and with our optimal filter.

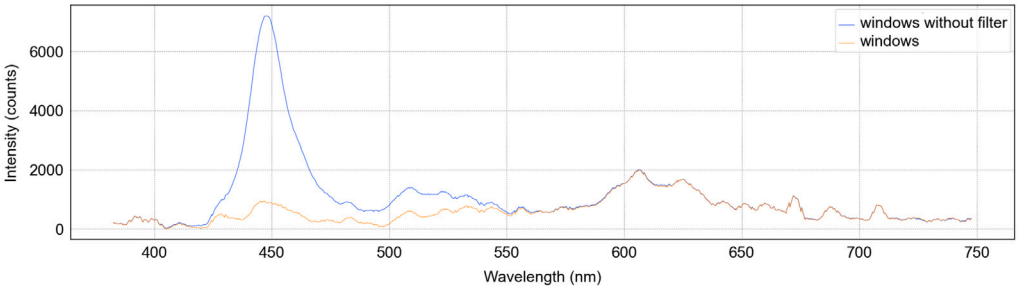

(c) Image projected in the Windows device Lenovo Yoga Pro 3 without filter and with our optimal filter.

Fig. 17. Irradiance spectrum of the same image projected in different devices. The projection is compared without filter and with our optimal filter.

The average processing time per image is on the order of hundredths of a second without parallelization. When applying basic parallelization across the algorithm tasks, this time is reduced by a factor of six, enabling a screen refresh rate of 85 Hz. With pixel-level parallelization, the filter could achieve even higher performance, which we identify as a meaningful direction for future research. These results suggest the filter's strong potential for integration into real-time video processing and future applications in electronic and wearable devices.

The filter's effectiveness is limited in white-dominant images, as white contains a significant amount of blue light. While the current design prioritizes contrast preservation, addressing the challenges posed by white-dominant images is a potential area for future research. Moreover, achieving the highest absorption levels can result in excessive color differences, which also warrants further investigation.

Processing performance should also be evaluated across a variety of devices with different screen technologies, taking into account the trade-offs between refresh rate, power consumption, and memory usage. We consider this an important direction for future research, particularly in the context of resource-constrained environments.

As we gain more insight into the effects of blue light on the brain and body, future research can be directed towards assessing the impact of filtering on these biological outcomes. We consider the proposed filter particularly suitable for head-mounted displays, which currently lack integrated blue light filtering mechanisms. Its application in assistive devices for individuals with visual impairments represents a promising direction for future work.

This work introduces a filter capable of adapting image colors and modulating intensity to suit user needs. It achieves high absorption rates while maintaining contrast, quality, and most colors, using a reduced color space to minimize blue emissions. The filter demonstrates reliable performance across different screens and devices, supported by physical light measurements obtained using a spectrophotometer. Furthermore, our results show that the filter can outperform existing solutions. These findings provide a promising foundation for its deployment across a wide range of electronic devices.

Declaration of competing interest

The authors declare the following financial interests/personal relationships which may be considered as potential competing interests: Maria Guijarro Mata-Garcia reports financial support was provided by Spain Ministry of Science and Innovation. Joaquin Recas Piorno reports financial support was provided by Spain Ministry of Science and Innovation. Maria Guijarro Mata-Garcia reports financial support was provided by UCM-ONCE-Tiflotechnology Chair. If there are other authors, they declare that they have no known competing financial interests or personal relationships that could have appeared to influence the work reported in this paper.

Acknowledgments

This work was partially supported by the Ministry of Science and Innovation, Spain (Grant no. PID2021-125596OB-I00 and PLEC2022-009261) and the UCM-ONCE-Tiflotechnology Chair, Spain.

Data availability

The test images used to obtain the results presented in this article are available at the following link: https://www.kaggle.com/datasets/juanbayonfernandez/landscape-test-images.

References

[1] V. Matouš, Analỳza vlivu modrého světla na lidského pozorovatele (B.S. thesis), České vysoké učenítechnické v Praze. Vypočetnía informačnícentrum., 2022.
[2] A. Singh, N. Verma, Exposure to Blue Light: A Regression in Child Development.
[3] J. Kumari, K. Das, M. Babaei, G.R. Rokni, M. Goldust, The impact of blue light and digital screens on the skin, J. Cosmet. Dermatol. 22 (4) (2023) 1185–1190.
[4] W.-J. Yeh, P.-T. Chien, Y.-T. Wen, C.-H. Wu, A comprehensive review of experimental models for investigating blue light-induced ocular damage: Insights into parameters, limitations, and new opportunities, Exp. Eye Res. (2024) 110142.
[5] M. Haghani, S. Abbasi, L. Abdoli, S.F. Shams, B.F.B.B. Zarandi, N. Shokrpour, A. Jahromizadeh, S.A. Mortazavi, S.M.J. Mortazavi, Blue light and digital screens revisited: A new look at blue light from the vision quality, circadian rhythm and cognitive functions perspective, J. Biomed. Phys. Eng. 14 (3) (2024) 213.
[6] F.A. Scheer, M.F. Hilton, C.S. Mantzoros, S.A. Shea, Adverse metabolic and cardiovascular consequences of circadian misalignment, Proc. Natl. Acad. Sci. 106 (11) (2009) 4453–4458.
[7] J.-X. Tao, W.-C. Zhou, X.-G. Zhu, Mitochondria as potential targets and initiators of the blue light hazard to the retina, Oxidative Med. Cell. Longev. 2019 (1) (2019) 6435364.
[8] R.G. Stevens, G.C. Brainard, D.E. Blask, S.W. Lockley, M.E. Motta, Adverse health effects of nighttime lighting: comments on American medical association policy statement, Am. J. Prev. Med. 45 (3) (2013) 343–346.
[9] E.M. Ward, D. Germolec, M. Kogevinas, D. McCormick, R. Vermeulen, V.N. Anisimov, K.J. Aronson, P. Bhatti, P. Cocco, G. Costa, et al., Carcinogenicity of night shift work, Lancet Oncol. 20 (8) (2019) 1058–1059.
[10] H.L. Mahoney, T.M. Schmidt, The cognitive impact of light: illuminating ipRGC circuit mechanisms, Nature Rev. Neurosci. 25 (3) (2024) 159–175.
[11] J. Kasowski, B.A. Johnson, R. Neydavood, A. Akkaraju, M. Beyeler, A systematic review of extended reality (XR) for understanding and augmenting vision loss, J. Vis. 23 (5) (2023) 5–5.
[12] P.V. Algvere, J. Marshall, S. Seregard, Age-related maculopathy and the impact of blue light hazard, Acta Ophthalmol. Scand. 84 (1) (2006) 4–15.
[13] K. Kim, A. Erickson, A. Lambert, G. Bruder, G. Welch, Effects of dark mode on visual fatigue and acuity in optical see-through head-mounted displays, in: Symposium on Spatial User Interaction, 2019, pp. 1–9.
[14] A. Erickson, K. Kim, A. Lambert, G. Bruder, M.P. Browne, G.F. Welch, An extended analysis on the benefits of dark mode user interfaces in optical see-through head-mounted displays, ACM Trans. Appl. Percept. (TAP) 18 (3) (2021) 1–22.
[15] F. Lux, Software to make your life better, 2015, https://justgetflux.com/.
[16] H.-P. Chiu, C.-H. Liu, The effects of three blue light filter conditions for smartphones on visual fatigue and visual performance, Hum. Factors Ergon. Manuf. Serv. Ind. 30 (1) (2020) 83–90.
[17] M.W. Driller, G. Jacobson, L. Uiga, Hunger hormone and sleep responses to the built-in blue-light filter on an electronic device: a pilot study, Sleep Sci. 12 (03) (2019) 171–177.
[18] J. Escofet, S. Bará, Reducing the circadian input from self-luminous devices using hardware filters and software applications, Light. Res. Technol. 49 (4) (2017) 481–496.
[19] J.A. Calvo-Sanz, C.E. Tapia-Ayuga, Blue light emission spectra of popular mobile devices: The extent of user protection against melatonin suppression by built-in screen technology and light filtering software systems, Chronobiol. Int. 37 (7) (2020) 1016–1022.
[20] M. Sroga, M. Dośpiał, M. Gacek, The effectiveness of eye protection application against harmful blue radiation in modern mobile devices, Acta Phys. Pol. A. 135 (2) (2019).
[21] S. Wahl, M. Engelhardt, P. Schaupp, C. Lappe, I.V. Ivanov, The inner clock—Blue light sets the human rhythm, J. Biophotonics 12 (12) (2019) e201900102.
[22] M. Ayaki, A. Hattori, Y. Maruyama, K. Tsubota, K. Negishi, Large-scale integration in tablet screens for blue-light reduction with optimized color: The effects on sleep, sleepiness, and ocular parameters, Cogent Biol. 3 (1) (2017) 1294550.
[23] A.D. Souchet, D. Lourdeaux, J.-M. Burkhardt, P.A. Hancock, Design guidelines for limiting and eliminating virtual reality-induced symptoms and effects at work: a comprehensive, factor-oriented review, Front. Psychol. 14 (2023) 1161932.
[24] L. Blue, Evaluation of fatigue and comfort of blue light under general condition and low blue light condition, in: Advances in Neuroergonomics and Cognitive Engineering: Proceedings of the AHFE 2019 International Conference on Neuroergonomics and Cognitive Engineering, and the AHFE International Conference on Industrial Cognitive Ergonomics and Engineering Psychology, July 24-28, 2019, Washington DC, USA, vol. 953, Springer, 2019, p. 411.
[25] Y. Tu, Y. Shi, L. Wang, Y. Zhang, Y. Yang, 17.2: invited paper: influence of blue light from smartphone on visual fatigue, in: SID Symposium Digest of Technical Papers, vol. 52, Wiley Online Library, 2021, pp. 108–111.
[26] N. Bansal, N.R. Prakash, J.S. Randhawa, P. Kalra, Effects of blue light on cognitive performance, Int. Res. J. Eng. Techmol. 4 (6) (2017) 2434–2442.
[27] H.-W. Chen, S.-L. Yeh, Effects of blue light on dynamic vision, Front. Psychol. 10 (2019) 414850.

[28] Y. Wei, Y. Zhang, Y. Wang, C. Liu, A study of the emotional impact of interior lighting color in rural bed and breakfast space design, Buildings 13 (10) (2023) 2537.
[29] S.Y. Kahu, R.B. Raut, K.M. Bhurchandi, Review and evaluation of color spaces for image/video compression, Color Res. Appl. 44 (1) (2019) 8–33.
[30] K. Masaoka, T. Yamashita, Y. Nishida, M. Sugawara, Color management for wide-color-gamut UHDTV production, SMPTE Motion Imaging J. 124 (3) (2015) 19–27.
[31] C. Headquarters, A Adobe® RGB (1998) Color Image Encoding, Adobe Systems Inc., San Jose, California, 2005.
[32] K. Otsuka, Color distribution plotter, 2023, https://www.mathworks.com/matlabcentral/fileexchange/69503-color-distribution-plotter.
[33] A. Mittal, R. Soundararajan, A.C. Bovik, Making a "completely blind" image quality analyzer, IEEE Signal Process. Lett. 20 (3) (2012) 209–212.
[34] N. Venkatanath, D. Praneeth, M.C. Bh, S.S. Channappayya, S.S. Medasani, Blind image quality evaluation using perception based features, in: 2015 Twenty First National Conference on Communications, NCC, IEEE, 2015, pp. 1–6.
[35] A. Mittal, A.K. Moorthy, A.C. Bovik, No-reference image quality assessment in the spatial domain, IEEE Trans. Image Process. 21 (12) (2012) 4695–4708.
[36] U. Bhaumik, F.B. Leloup, K. Smet, Systematic comparison of head mounted display colorimetric performance using various color characterization models, Opt. Contin. 2 (6) (2023) 1490–1504, http://dx.doi.org/10.1364/OPTCON.493238, URL https://opg.optica.org/optcon/abstract.cfm?URI=optcon-2-6-1490.
[37] A. Rougetet, Landscape pictures, 2020, https://www.kaggle.com/datasets/arnaud58/landscape-pictures.
[38] Anonymous, Landscape test images, 2025, Removed for blind review.
[39] A.K. Tripathi, S. Mukhopadhyay, A.K. Dhara, Performance metrics for image contrast, in: 2011 International Conference on Image Information Processing, IEEE, 2011, pp. 1–4.
[40] R. Narayanam, K.K. Kumar, Int. J. Eng. Sci. Res. Technol. Novel Exp. Eval. Dev. Novel Stand. Notion Image Qual. Assess. (iqa) Measures Comput. Time Image Contrast.
[41] Z. Wang, Image quality assessment: Form error visibility to structural similarity, IEEE Trans. Image Process. 13 (4) (2004) 604–606.
[42] W. Xue, L. Zhang, X. Mou, A.C. Bovik, Gradient magnitude similarity deviation: A highly efficient perceptual image quality index, IEEE Trans. Image Process. 23 (2) (2013) 684–695.
[43] D.B. Moyano, S.B. Moyano, M.G. López, A.S. Aznal, R.A. González L, Photometric and colorimetric analysis of light emitting diode luminaires for interior lighting design, Color Res. Appl. 46 (4) (2021) 791–807.